Effect of Prone Positioning on Pathophysiology and Lung Histopathology During VV-ECMO in Severe ARDS: An Experimental Animal Study

Enric Barbeta[1,2,3] Blanca Llonch[2], Jordi Vallverdú[1,2], Kasra Kiarostami[2], Luigi Zattera[1,2], Roberto Cabrera[2], Flavia Galli[2], Laia Fernández-Barat[2,3], Ana Motos[2,3,4], Filippo Sartori[5], Lisa Persico[6], Federico Carpenteri[7], Lucia Alessandra Pasqua[8], Nona Rovira-Ribalta[2], Cristina Miralles[9], Guillermo Laguna[1], Albert Carramiñana[1], Eduard Argudo[10], Maria Martínez-Martínez[10], Elisabet Gallart[10], Juan Antonio Sánchez[11], Katalin Rubí[12], Elena Sandoval[12], Maite Mata[12], Federica Piedepalumbo[13], Davide Calabretta[2,14], Carlos Ferrando[1,2,3*], Jordi Riera[10*], Antoni Torres[2,3*].

1. Surgical ICU, Anesthesiology, Hospital Clínic de Barcelona, Barcelona, Spain.
2. Institut d'Investigacions August Pi i Sunyer, Universitat de Barcelona, Barcelona, Spain.
3. Centro de Investigación Biomédica en Red de Enfermedades Respiratorias, Insituto de Salud Carlos III.
4. University of Nantes, Nantes, France.
5. Department of Medicine, Respiratory Medicine Unit, University of Verona and Azienda Ospedaliera Universitaria Integrata of Verona, Verona, Italy.
6. Anesthesiology and Intensive Care Medicine, Department of Medical and Srugical Specialties, Radiological Sciences and Public Health, University of Brescia, Brescia, Italy.
7. Università Cattolica del Sacro Cuore, Rome, Italy.

8. Anaesthesia and Intensive Care, Department of Medical and Srugical Sciences, Magna Graecia University, Catanzaro, Italy.
9. Pathological Anatomy, Hospital Clínic de Barcelona, Barcelona, Spain.
10. Department of Critical Care, Vall d'Hebron University Hospital and Vall d'Hebron Research Institute, Barcelona, Spain.
11. Department of Intensive Care Medicine, Hospital Universitario de La Princesa, Madrid, Spain.
12. Cardiovascular Surgery Department, Hospital Clínic de Barcelona, Barcelona, Spain.
13. Respiratory Unit and Cystic Fibrosis Adult Center, Fondazione IRCCS Ca' Granda Ospedale Maggiore Policlinico, Milan, Italy.
14. Department of Anesthesia and Critical Care, ASST Ovest Milanese, Ospedale Civile di Legano, Milan, Italy.

Corresponding author

Antoni Torres, MD, PhD

University of Barcelona, Barcelona, Spain.

atorres@recerca.clinic.cat

-ONLINE DATA SUPPLEMENT-

ADDITIONAL METHODS

All procedures were conducted following the European Directive 2010/63/UE and Spanish RD 53/2013 regulations related to the Guide for the Care and Use of Laboratory Animals and complied with the PREPARE and ARRIVE guidelines.

Animal preparation

Eight female domestic pigs (Large White - Landrace) were premedicated via intramuscular administration of midazolam (0.17 mg/Kg), xylazine (4 mg/Kg) and ketamine (6 mg/Kg); and received antimicrobial (ceftriaxone (75mg/kg)) and antithrombotic prophylaxis (40 mg enoxaparin). Following cannulation of an auricular vein, anaesthesia was induced with an intravenous bolus of propofol (2 mg/kg) to facilitate orotracheal intubation. General anaesthesia was maintained throughout the surgical preparation via continuous intravenous infusion of propofol (2-5 mg/kg/h), fentanyl (5-10 µg/kg/h) and midazolam (0.1-0.3 mg/kg/h). During surgical preparation, a tidal volume of 6 mL/kg, respiratory rate of 20 breaths/min, inspiratory-to-expiratory ratio (I:E) of 1:2, PEEP of 4 cmH_2O, and FiO_2 of 0.40 were used. A urinary catheter and an esophageal balloon catheter (NutriVent™, SIDAM S.R.L., Italy) were inserted. The FluxMed (MBMed, Buenos Aires, Argentina) monitor, which includes a pneumotachograph placed between the endotracheal tube and the “Y” piece of the breathing circuit, a pressure channel to measure esophageal pressure, and a mainstream infrared CO_2 sensor (Capnostat 5, Respironics, Wallingford, CT, USA), was used. Size S electrical impedance tomography belts (Timpel, São Paulo, Brazil) were also positioned. A

pulmonary artery catheter (Arrow E3 International, USA) was inserted via the left external jugular vein through an 8 Fr introducer and advanced into the pulmonary artery under pressure waveform guidance. The left femoral artery was cannulated with a 5 Fr arterial catheter for advanced hemodynamic monitoring (PiCCO®, Getinge, Sweden). PiCCO calibration was performed using the mean of three 10 mL iced saline injections prior to each set of measurements. All hemodynamic parameters were obtained after calibration to atmospheric pressure at the mid-thoracic level. All vascular access was achieved via ultrasound-guided puncture.

ARDS model induction

A recently developed animal model of severe ARDS pneumonia was used (1). The study was conducted in female Large White-Landrace pigs subjected to up to 110 hours of mechanical ventilation (SERVO-U, Maquet, NJ, USA). To induce severe ARDS, animals were subjected to 3 hours of ventilator-induced lung injury using a driving pressure of 32 cmH_2O and zero positive end-expiratory pressure (PEEP), resulting in a harmful dynamic pulmonary strain greater than 1.5 (2). Following this, 15 mL of 10^7 colony-forming units (CFU)/mL of multidrug-resistant *Pseudomonas aeruginosa*—susceptible to both meropenem and levofloxacin—was instilled into each lung lobe via bronchoscopy.
Pneumonia was clinically diagnosed based on a decrease in PaO_2 relative to baseline, or hypotension requiring phenylephrine, plus at least one of the following signs of infection: body temperature >38.5 °C, white blood cell count $>14 \times 10^9$/L, or purulent secretions. Upon pneumonia diagnosis, antimicrobial therapy was initiated with 25 mg/kg of meropenem every 8 hours and 10 mg/kg

of levofloxacin every 24 hours until the end of the experiment. 15mg/kg every 12 hours of vancomycin was also started as prophylaxis. After bacterial challenge, injurious mechanical ventilation was resumed using the same previous settings, except for the addition of a PEEP of 3 cmH_2O. Driving pressure could be temporarily reduced to 23 cmH_2O in cases of severe hemodynamic instability due to significant variations in venous return caused by large tidal volumes. ARDS was diagnosed when the PaO_2/FiO_2 < 100 mmHg. Once ARDS was established, animals were ventilated in prone position using a lung-protective strategy. Driving pressure was set at 14 cmH_2O, PEEP at 10 cmH_2O, and respiratory rate was adjusted to maintain normocapnia. Cisatracurium (1–3 mg/kg/h) was administered to all animals.

Extracorporeal support

In all animals, a 21 Fr drainage cannula (Getinge, Sweden) was inserted in the right femoral vein, and a 15–17 Fr reinfusion cannula (Getinge, Sweden) was placed in the right external jugular vein. Extracorporeal support was provided using a Cardiohelp system (Getinge, Sweden) equipped with a centrifugal pump and a Quadrox PLS membrane lung (Maquet; surface area 1.8 m^2). After cannulation, catheters were connected to the extracorporeal circuit. An initial bolus of unfractionated heparin (200–250 U/kg) was administered in both groups immediately following cannula placement. A continuous infusion of heparin was subsequently maintained and titrated according to activated partial thromboplastin time (aPTT, 40-60 seconds).

Organ support

During VV-ECMO, analgosedation and neuromuscular block was maintained with high doses of propofol (5mg/kg/h), midazolam (0.3mg/kg/h), and fentanyl (10 µg /kg/h) to enable cisatracurium (1-3 mg/kg/hr) infusion. Sepsis-induced hypotension (mean arterial pressure <65mmHg) was treated with phenylephrine (0 – 2 µg /kg/min), and vasopressin at 0.03 IU/min was added when phenylephrine dose exceeded 0.3mcg/kg/min. In case of persistent hypotension with >1mcg/kg/min of phenylephrine and 0.03 UI/min of vasopressin, hydrocortisone was administered at a dose of 50mg / 6 hours. Crystalloids or glucose 5% were infused at a 100ml/hr. Furosemide bolus (10-20 mg) were administered to reach a urinary output of >1ml/kg/hr. Fever (>38 Cº) was treated with 1gram / 8 hours and with cold blankets and ice. Hypothermia (<36 Cº) was treated with external heating.

Stopping rules

The experiment was discontinued if any of the following occurred: pH < 7.1; PaO_2/FiO_2 <50; active bleeding; shock with a mean arterial pressure < 60 mmHg despite phenylephrine > 2 µg/kg/min and vasopressin at 0.03 IU/min; haemoglobin < 5 g/dL; cardiac arrest lasting > 1 minute; failure of cannulation; circuit thrombosis; or pneumothorax.

Calculation of physiological variables

Variable	**Unit**	**Formula**
Shunt Fraction (Qs/Qt)	%	$Qs/Qt = (CcO_2 – CaO_2)/(CcO_2 - CvO_2)$
Physiological dead space (Enghoff) (Vd/Vt)	%	$Vd/Vt = (PaCO_2 - PECO_2)/PaCO_2$
Cardiac output (CO)	L/min	CO = HR * SV
Native lung O_2 consumption (VO_{2NL})	mL/min	$VO_{2NL} = CO * (CaO_2 – CvO_2)$
Membrane Lung O_2 consumption (VO_{2ML})	mL/min	VO_{2ML} = flow ML * ($C_{postML} O_2 - C_{preML} O_2$)
VO_2 total	mL/min	$VO_{2ML} + VO_{2NL}$
Native lung CO_2 elimination (VCO_{2NL})	mL/min	VCO_2 per breath * respiratory rate
Membrane lung CO_2 elimination (VCO_{2ML})	mL/min	$VCO_{2ML} = 0.8 * (VO_{2ML} + VO_{2NL}) − VCO_{2NL}$.

VCO_2 total	mL/min	$VCO_{2ML} + VCO_{2NL}$
Driving pressure (ΔP)	cmH_2O	ΔP = Pplat - PEEP
Respiratory system compliance (Crs)	mL/cmH_2O	Crs = VT / ΔP
Lung compliance (C_L)	mL/cmH_2O	C_L = VT / [ΔP - (iPes – ePes)]
Chest wall compliance (C_{CW})	mL/cmH_2O	C_{CW} = VT / (iPes – ePes)
End-inspiratory transpulmonary pressure (P_L)	cmH_2O	P_L = Pplat * (E_L/E_{RS})
Systemic vascular resistance (SVR)	$dyn \cdot s/cm^5$	SVR = (MAP – CVP) / CO * 80
Pulmonary vascular resistance (PVR)	$dyn \cdot s/cm^5$	PVR = (MPAP – PCWP) / CO * 80
Respiratory quotient (RQ)	-	RQ = VCO_2/VO_2 = 0.8

Abbreviations: CaO_2: arterial oxygen content; **CcO_2:** capillary oxygen content; **cmH_2O:** centimetres of water; **CO:** cardiac output; **CO_2:** carbon dioxide; **CVP:** central venous pressure; **CvO_2:** mixed venous oxygen content; **C_{cw}:** chest wall distensibility; **C_L:** lung distensibility; **Dyn:** dynes **ΔP:** driving pressure; **Crs:** respiratory system compliance; **E_L:** lung elastance; **ePes:** esophageal pressure at the end of expiration; **E_{rs}:** respiratory system elastance; **FiO_2:** fraction

of inspired oxygen; **HR:** heart rate; **iPes:** esophageal pressure at the end of inspiration; **MAP:** mean arterial pressure; **min:** minute; **ML:** membrane lung; **mL:** milliliters; **mmHg:** millimeters of mercury; **MPAP:** mean pulmonary arterial pressure; **NL:** native lung; **O_2:** oxygen; **OX:** oxygenator; **$PaCO_2$:** arterial partial pressure of carbon dioxide; **PCWP:** pulmonary capillary wedge pressure; **$PECO_2$:** mixed expired carbon dioxide; **PEEP:** positive end-expiratory pressure; **Pplat:** positive end-inspiratory plateau pressure; **P_L:** transpulmonary pressure; **PVR:** pulmonary vascular resistances **Qs:** shunt cardiac output; **Qt:** total cardiac output; **RQ:** respiratory quotient; **SV:** end-systolic volume; **SvO2:** central venous saturation of oxygen; **SVR:** systemic vascular resistance; **P_L:** transpulmonary pressure; **Vd/Vt:** physiological dead space; **VCO_2:** carbon dioxide elimination; **VO_2:** oxygen consumption; **TV:** tidal volume.

Sample processing

Wet-to-dry lung weight ratio: Samples of approximately 10 g were excised and immediately weighed (wet weight), then dried in an oven at 60 °C for 72 h to obtain the dry weight, from which the wet-to-dry weight ratio was calculated.

Histopathology: The most affected region of each pulmonary lobe was sampled for histological studies. Samples for histopathology were fixed in formalin and dissected to obtain tissue fragments approximately 2 cm in length and 0.3 cm in thickness. These were placed into cassettes for subsequent dehydration through a graded series of alcohols, followed by paraffin embedding to solidify the tissue. Paraffin blocks were then prepared and sectioned at a thickness of 2 micrometres using a microtome. The sections were mounted onto glass slides and stained with the standard histological stain, Hematoxylin and Eosin (H&E). Finally, coverslips were applied to the slides to protect the tissue and facilitate microscopic examination.

ATS Lung Injury Score

Parameter	0	1	2
A. Neutrophils in the alveolar space	none	1–5	>5
B. Neutrophils in the interstitial space	none	1–5	>5
C. Hyaline membranes	none	1	>1
D. Proteinaceous debris filling the airspaces	none	1	>1
E. Alveolar septal thickening	<2×	2×–4×	>4×

Score = [(20 × A) + (14 × B) + (7 × C) + (7 × D) + (2 × E)] / (number of fields × 100)

Microbiology: Bronchoalveolar lavage was performed in the right upper lobe using three 10-mL aliquots of sterile saline solution. For lung tissue analyses, the most affected region of each pulmonary lobe was sampled. Quantitative cultures of *Pseudomonas aeruginosa in* MacConkey agar were performed using standard methods (3). Ultimately, *Pseudomonas aeruginosa* was identified by mass spectrometry through a Microflex LT (BrukerDaltonics GmbH, Leipzig, Germany) and *Pseudomonas aeruginosa* identification was performed using the MALDI BioTyper 2.0 software (BrukerDaltonics). Pneumonia diagnosis in tissue samples was defined as quantitative *Pseudomonas aeruginosa* lobar culture ≥ 3 log CFU/g.

Electrical impedance tomography

Electrical impedance tomography, by applying small imperceptible electrical currents, can detect changes in lung ventilation. An electrode belt was placed around the 4th–6th intercostal spaces, and the electrical impedance tomograph (Enlight 1800, Timpel Medical, São Paulo, Brazil) was used to acquire and reconstruct the electrical impedance tomography (EIT) signals. EIT data were recorded at a frame rate of 50 Hz, and each frame was represented as a 32 × 32 pixel matrix (1,024 pixels). The raw data were post-processed to reduce noise and exclude non-pulmonary signals (e.g., heart and chest wall), according to the manufacturer's algorithm based on anthropometric data. The processed data were then analysed using dedicated software packages (Timpel File Convert, Timpel Offline Analysis, and Timpel Trends Tool®; Timpel Medical, São Paulo, Brazil). In this study, both global and regional components of electrical tomography impedance-derived variables were analysed, namely end-

expiratory lung impedance (EELZ), impedance-derived compliance, and tidal impedance (ΔZ). EELZ, expressed in arbitrary units (AU), represents the electrical impedance measured at end-expiration and reflects changes in end-expiratory lung volume over time. Impedance-derived compliance, reported in AU/cmH_2O, is a surrogate of lung compliance calculated as the ratio between tidal impedance variation (ΔZ) and the corresponding change in airway pressure, representing the impedance change per unit of pressure. ΔZ, expressed in AU, corresponds to the impedance variation between end-inspiration and end-expiration during a single respiratory cycle and is closely related to the tidal volume distribution. These variables were evaluated globally for the entire lung and regionally by distinguishing anterior and posterior lung regions, which were considered non-dependent and dependent in the supine position, and dependent and non-dependent in the prone position, respectively.

ADDITIONAL RESULTS

Wet-to-Dry Lung Weight Ratio and ATS lung injury score in Animals Completing the 48-Hour Intervention

When non-dependent and dependent regions were analysed including only animals that completed the 48-hour intervention, median values were slightly higher in the prone position group (7.84 [7.39–8.28]) than in the supine position group (6.70 [6.26–7.76]). As in the primary analysis, the distribution pattern differed between positions, with the prone position showing higher values in dependent regions and greater heterogeneity across lung areas. Two-way repeated-measures ANOVA revealed no significant overall differences between groups ($p = 0.50$) or regions ($p = 0.38$), but a significant group-region interaction ($p = 0.048$), indicating that regional behavior depended on position. In the prone position group, dependent regions had higher values (8.17 (8.04–9.09)) than non-dependent regions (7.08 (6.17–7.98)) ($p = 0.041$), whereas no such difference was observed in the supine group (dependent 6.70 (6.31–8.98) vs. non-dependent 6.70 (6.25–7.44); $p = 0.47$).

When ratios between non-dependent and dependent regions were compared, the median ratio was lower in the prone position group (0.82 (0.79–0.85)) than in the supine position group (0.98 (0.86–1.00)), consistent with a steeper regional gradient in prone animals, although this difference was not statistically significant ($p = 0.29$).

Regarding the ATS lung injury score, when the analysis was extended to individual lobes, no global differences were observed between groups ($p = 0.38$), but significant effects of lobe ($p = 0.002$) and group - lobe interaction ($p =$

0.021) were found. We found higher values in the right middle lobe in the prone position group compared to the supine group (0.55 (0.50–0.60) vs. 0.30 (0.26–0.42); p = 0.041) and higher values in the right lower lobe in the supine group compared to the prone group (0.59 (0.53–0.67) vs. 0.23 (0.19–0.27); p = 0.012), with no significant differences in the remaining lobes.

Table E1. Median values of hemodynamic variables during extracorporeal support.

	Prone Position (n = 4)	Supine Position (n = 4)	p value
Mean pulmonary arterial pressure, mmHg	35 (31.21 - 35.05)	30.75 (28.50 - 33.88)	0.61
Mean arterial pressure, mmHg	79.25 (70.75 - 88.75)	82.25 (77.63 - 88.75)	0.41
Wedge pressure, mmHg	16.33 (16.13 - 18)	15.33 (15 - 16.63)	0.43
Central venous pressure, mmHg	11 (10 - 11.50)	12.50 (8.88 - 12.88)	0.84
Cardiac output, lpm	5.55 (5.19 - 6.18)	5.67 (5.44 - 6.07)	0.78
Pulmonary vascular resistance (dyn·s/cm^{-5})	290.30 (232.10 - 329.60)	218 (192 - 271.70)	0.75
Systemic vascular resistance (dyn·s/cm^{-5})	991.80 (740.70 - 1049)	898.50 (808 - 938)	0.85

Vasopressor dependency index	0.05 (0 - 3.04)	0.18 (0.07 - 0.36)	0.26

Results are presented as median (IQR) across all timepoints. Statistical analyses were performed using a mixed-effects model; p values correspond to the group effect. Significant time effects within the model are denoted by †: $p < 0.05$ (†), $p < 0.01$ (††), and $p < 0.001$ (†††).

Abbreviations. cm: centimeter; lpm: liters per minute; mmHg: millimeters of mercury; dyn: dynes; s: second.

Table E2. Median values of extracorporeal support–related variables.

	Prone Position (n = 4)	Supine Position (n = 4)	p value
Pre-pump pressure, mmHg	-71.25 [(-76.25 – (-69.63)]	-64.25 [(-66.25 – (-63.63)]	0.29
Sweep flow, lpm	6 (5.56 – 6.87)	6.62 (5.56 – 8.06)	0.92
ECMO circuit flow, lpm	3.22 (3.14 – 3.52)	3.23 (3.09 – 3.29)	0.53
Pre-membrane pressure, mmHg	165 (150 – 170)	168.80 (158.60 – 171)	0.64
Post-membrane pressure, mmHg	174.40 (160 – 169.1)	163.10 (158.50 – 171.30)	0.69†

Results are presented as median (IQR) across all timepoints. Statistical analyses were performed using a mixed-effects model; p values correspond to the group effect. Significant time effects within the model are denoted by †: $p < 0.05$ (†), $p < 0.01$ (††), and $p < 0.001$ (†††).

Abbreviations. lpm: liters per minute; mmHg: millimeters of mercury; VV-ECMO: venou-venous extracorporeal membrane oxygenation.

Figure E1

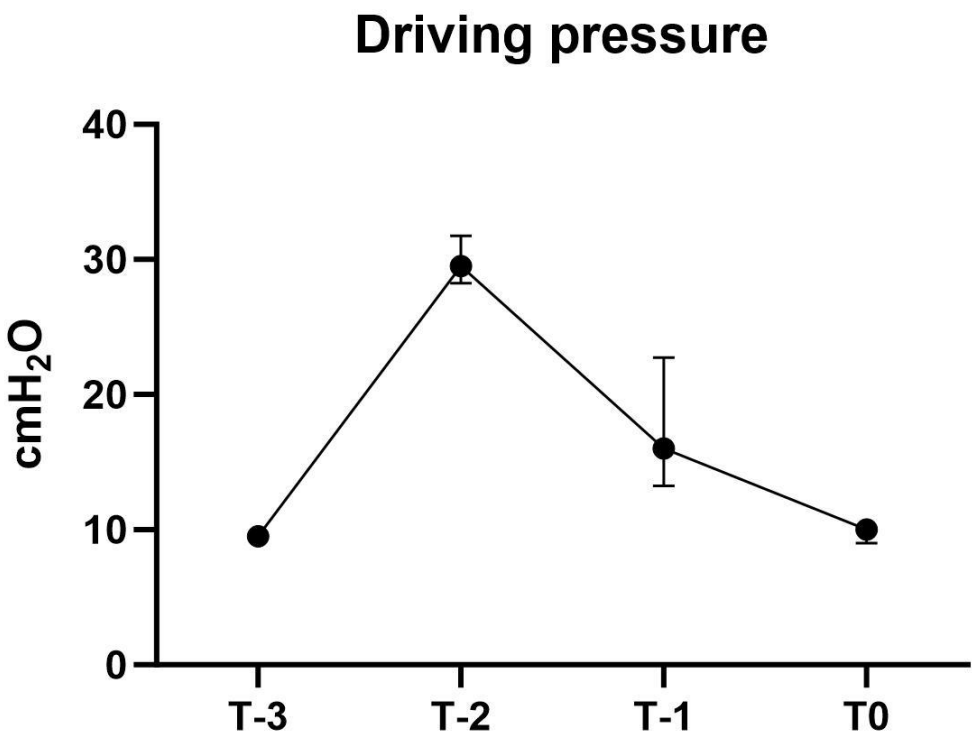

Figure E2

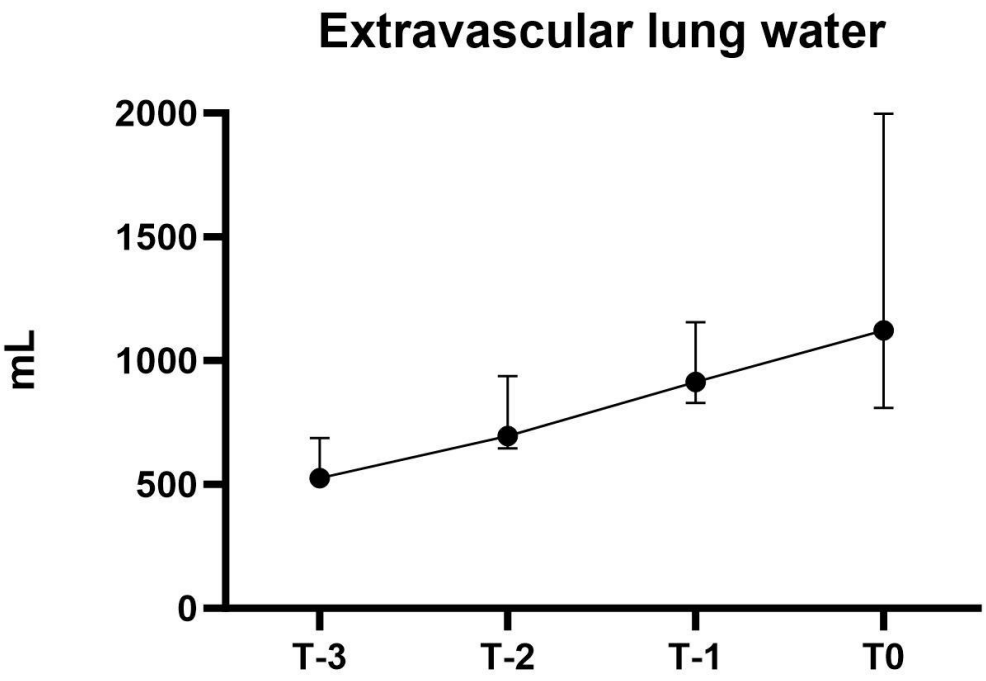

Figure E3

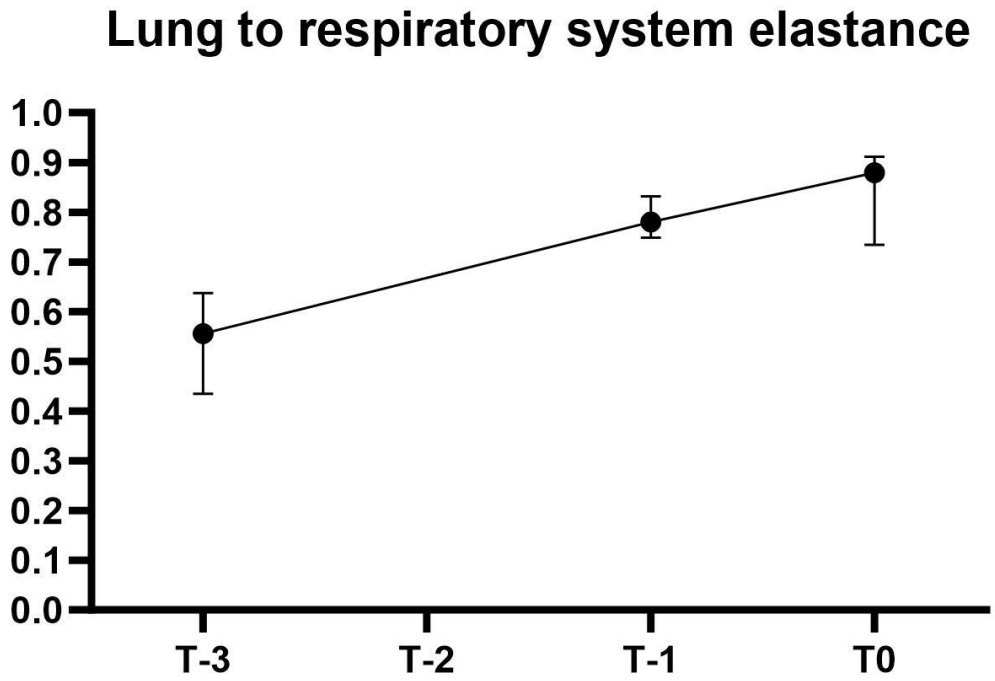

Figure E4

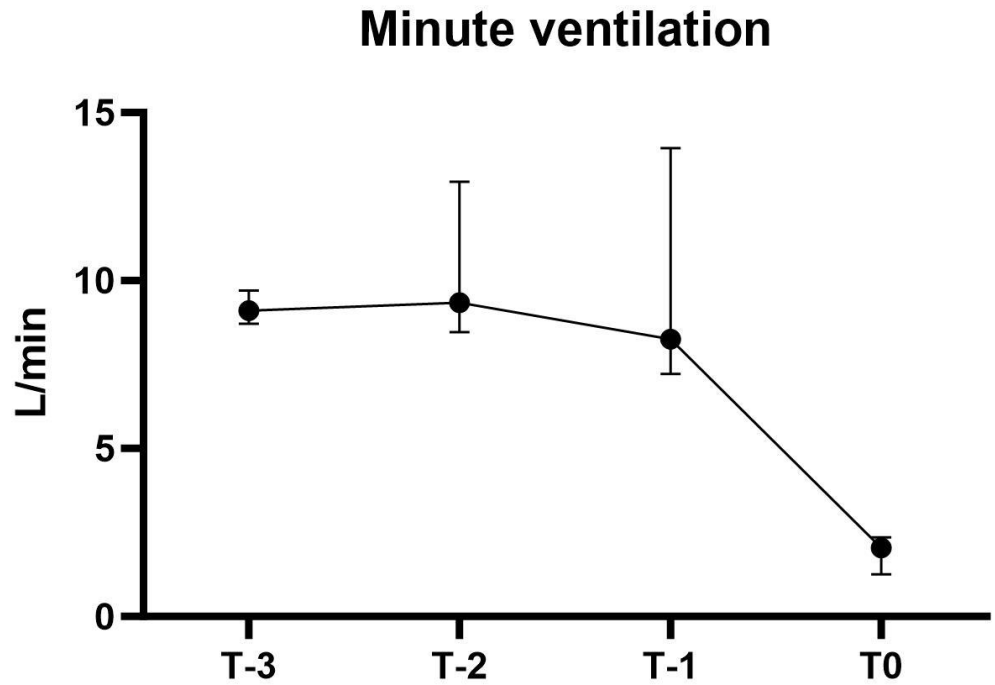

Figure E5

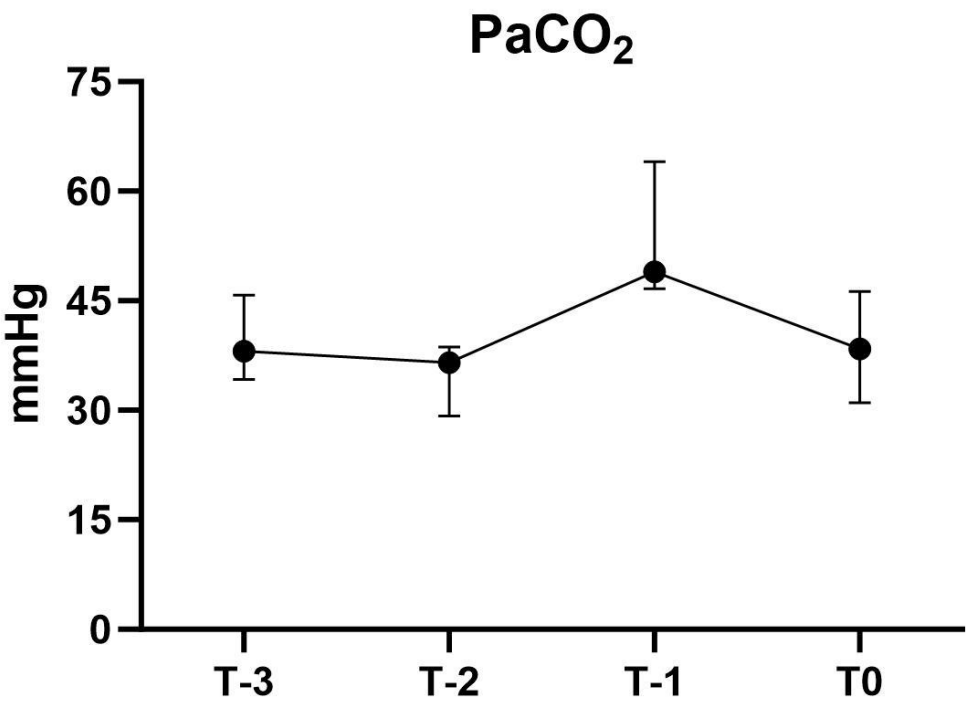

Figure E6

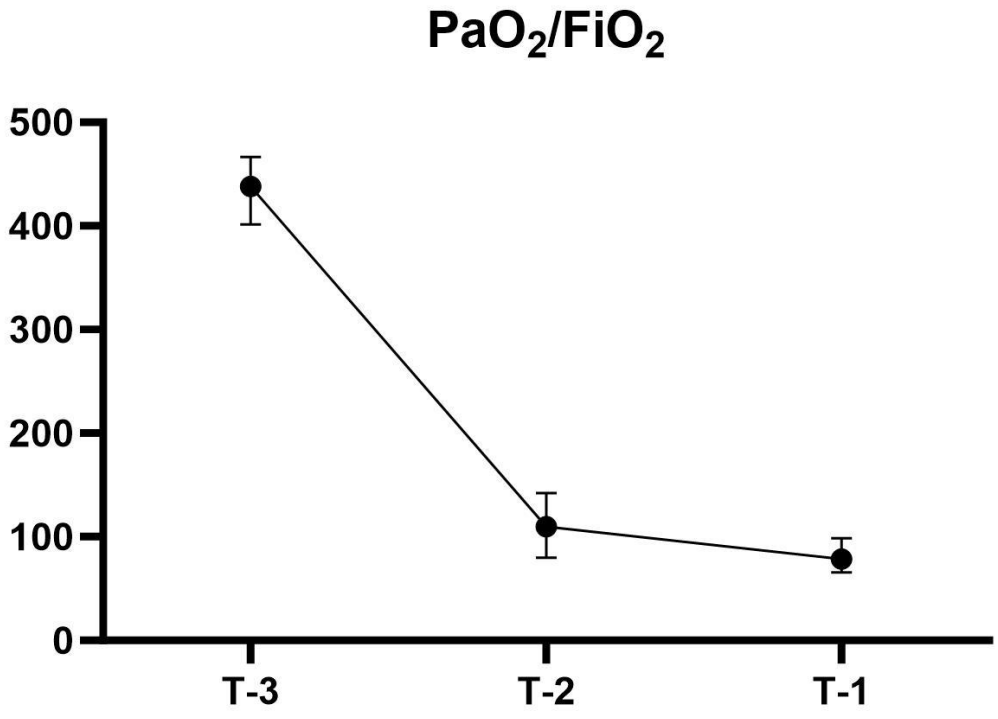

Figure E7

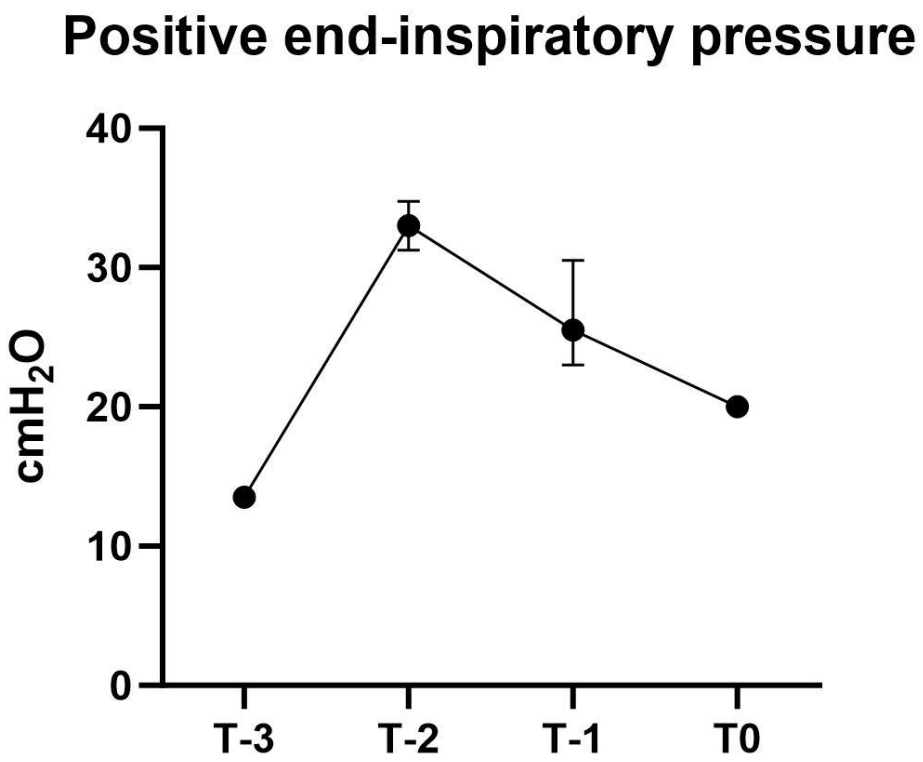

Figure E8

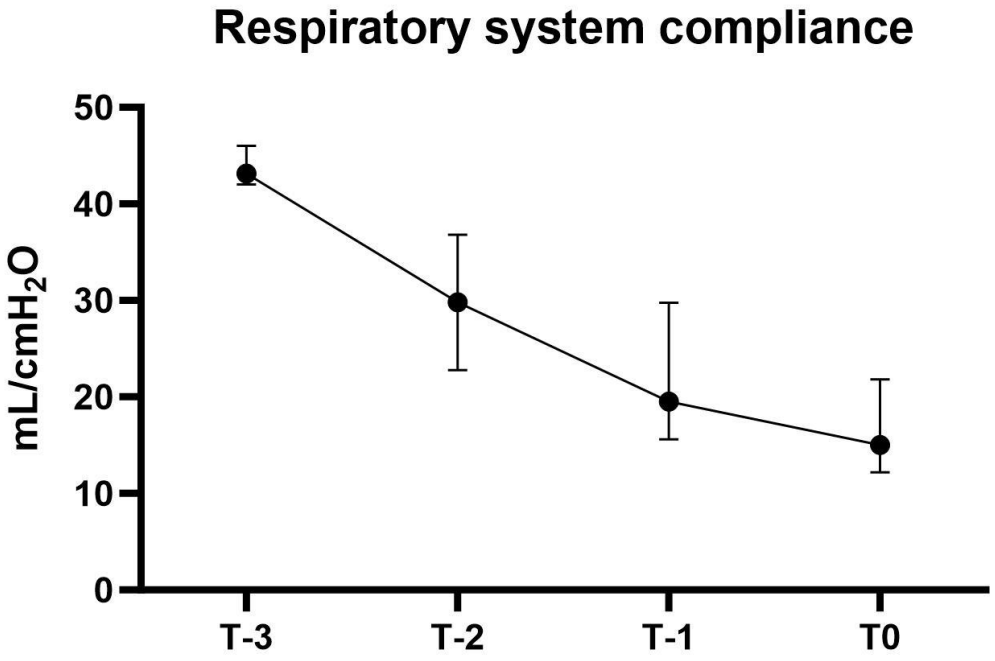

Figure E9

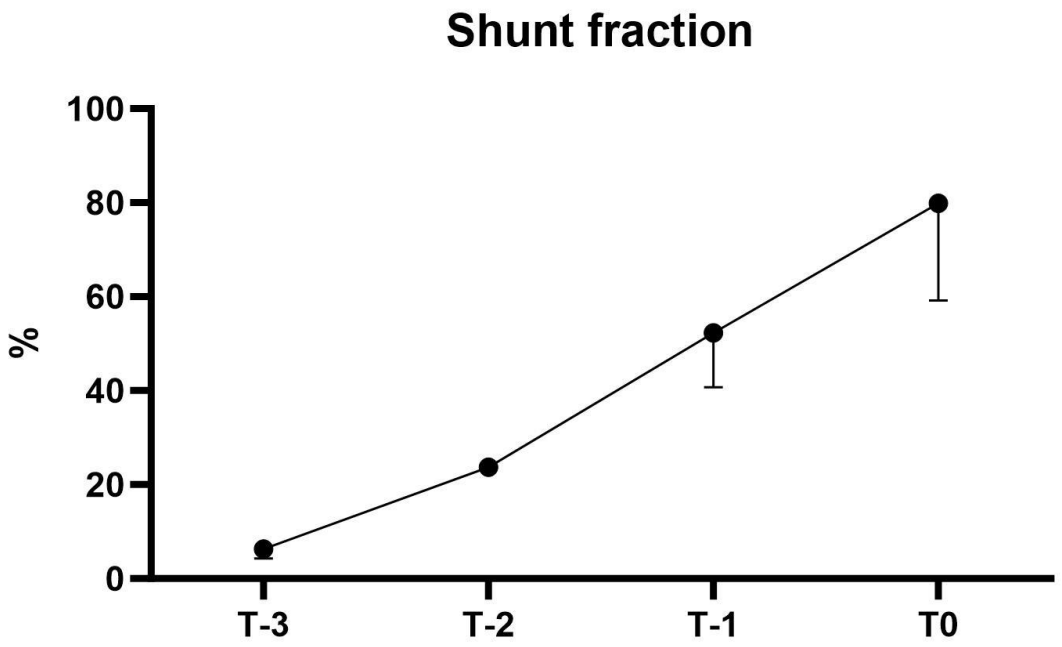

Figure E10

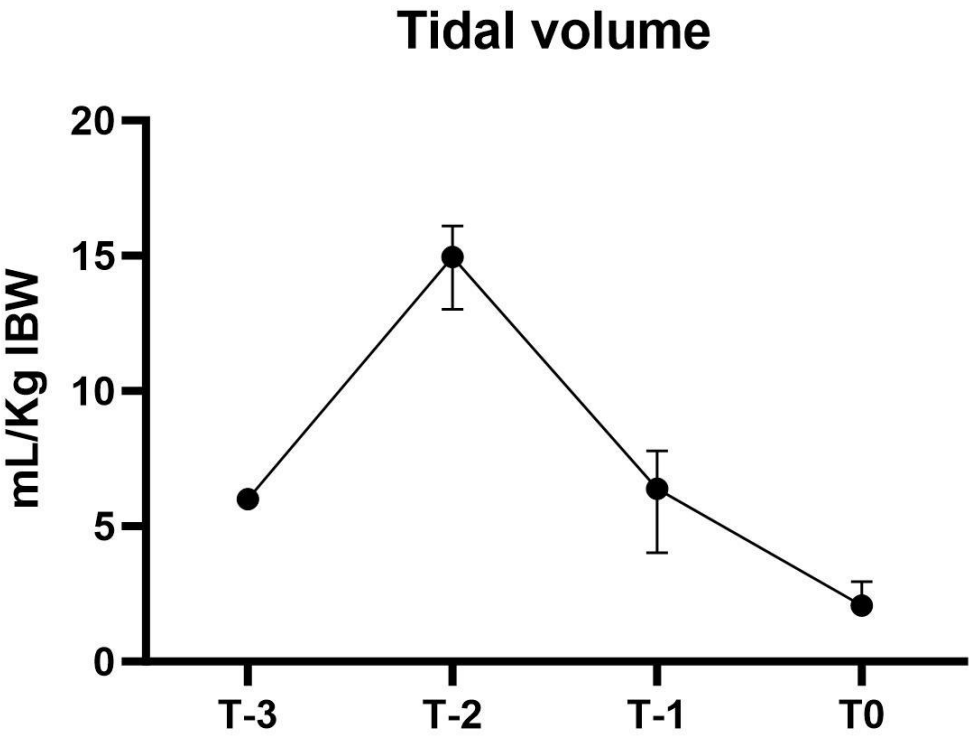

Figure E11

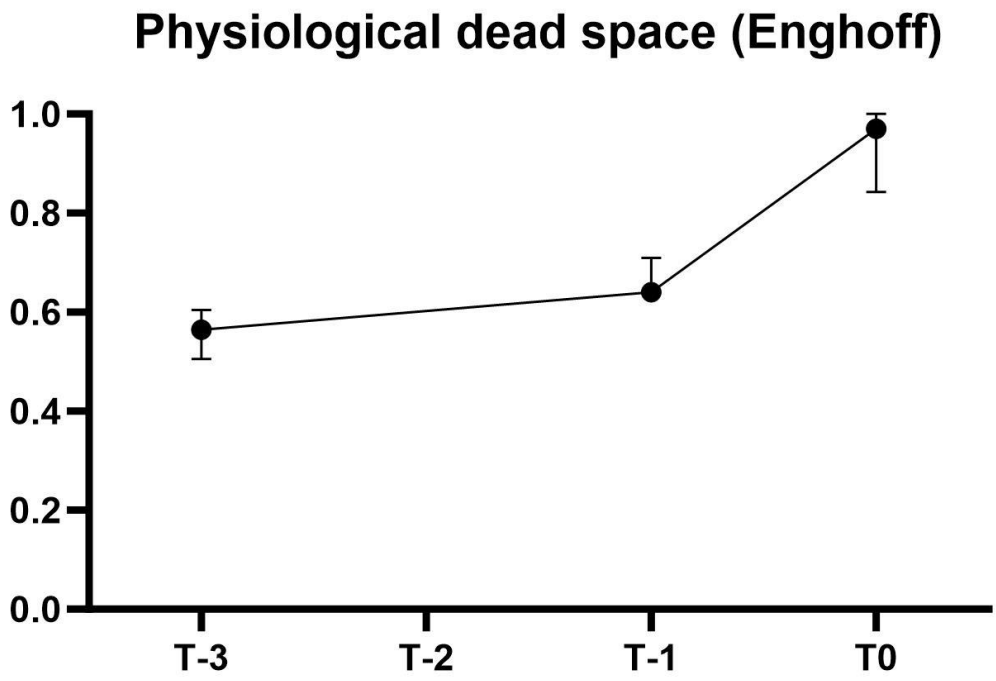

Figure E12

A

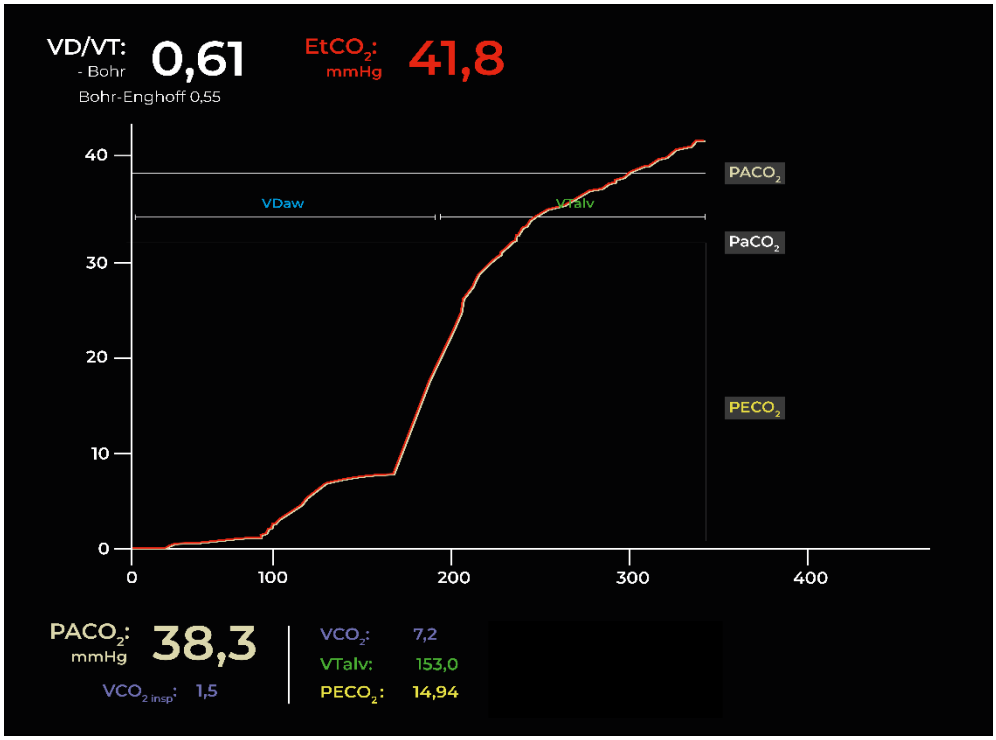

B

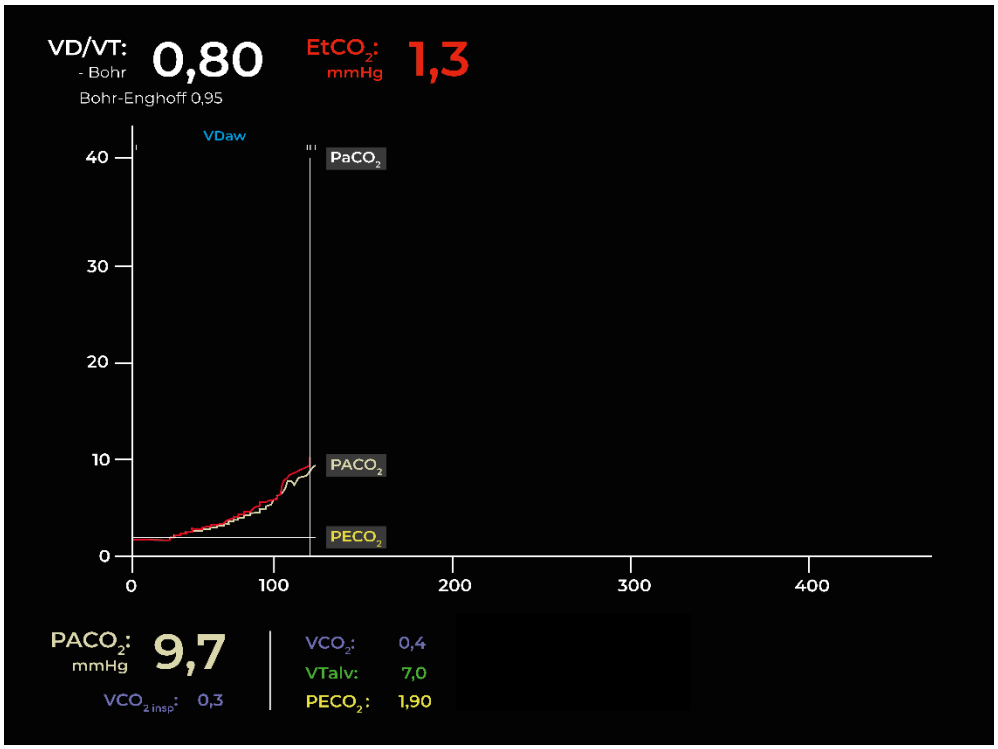

C

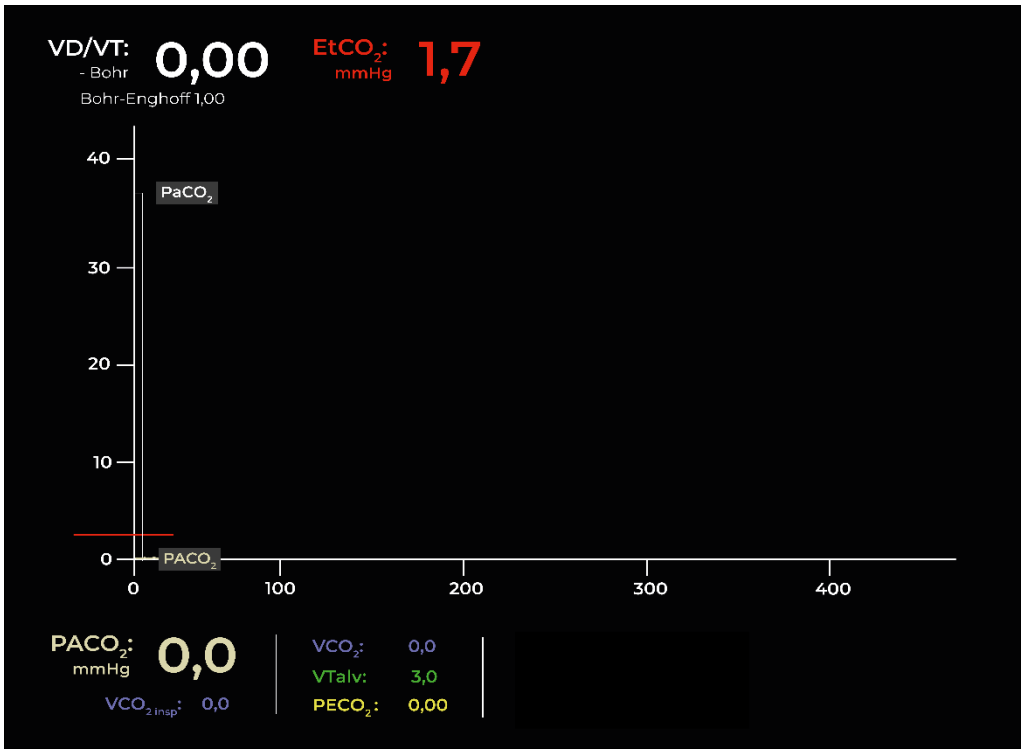
VD/VT:
0,00
- Bohr
Bohr-Enghoff 1,00
EtCO2:
mmHg
1,7
40
30
20
10
0
PaCO2
PACO2
0
100
200
300
400
PACO2:
mmHg
0,0
VCO2 insp: 0,0
VCO2: 0,0
VTalv: 3,0
PECO2: 0,00

Figure E13

A: Prone position

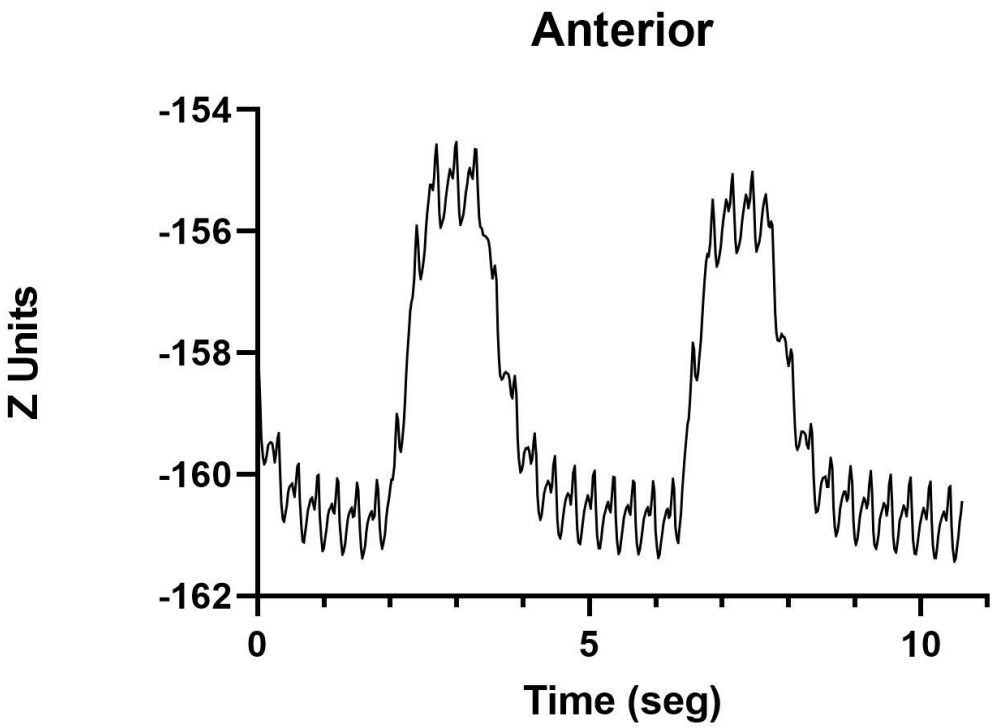

B: Supine position

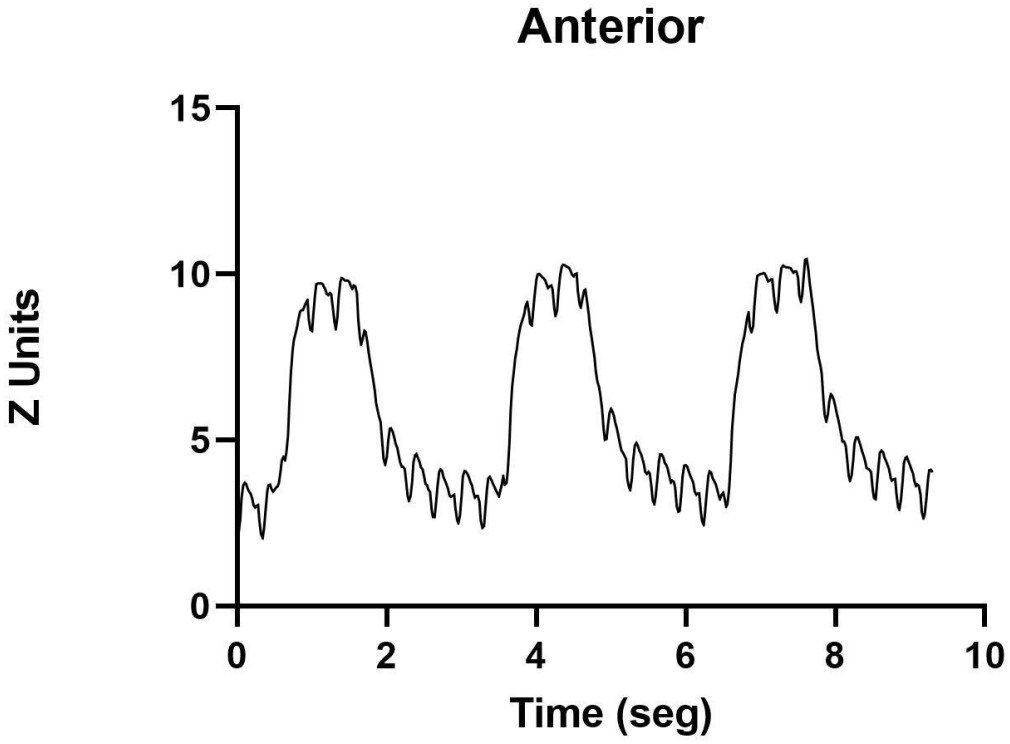

C: Prone position

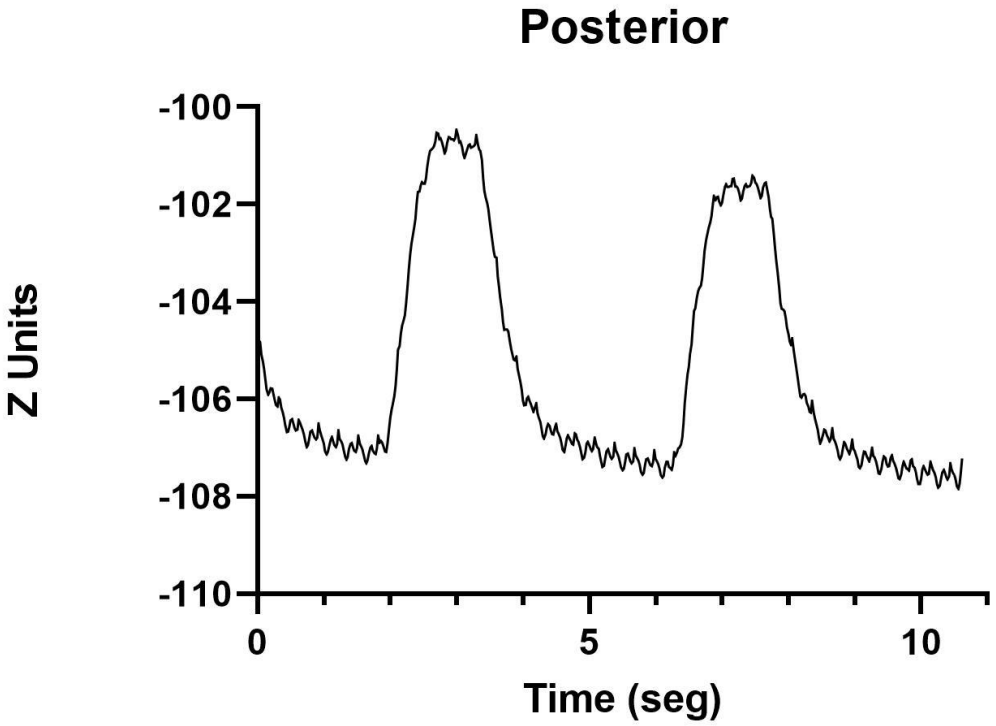

D: Supine position

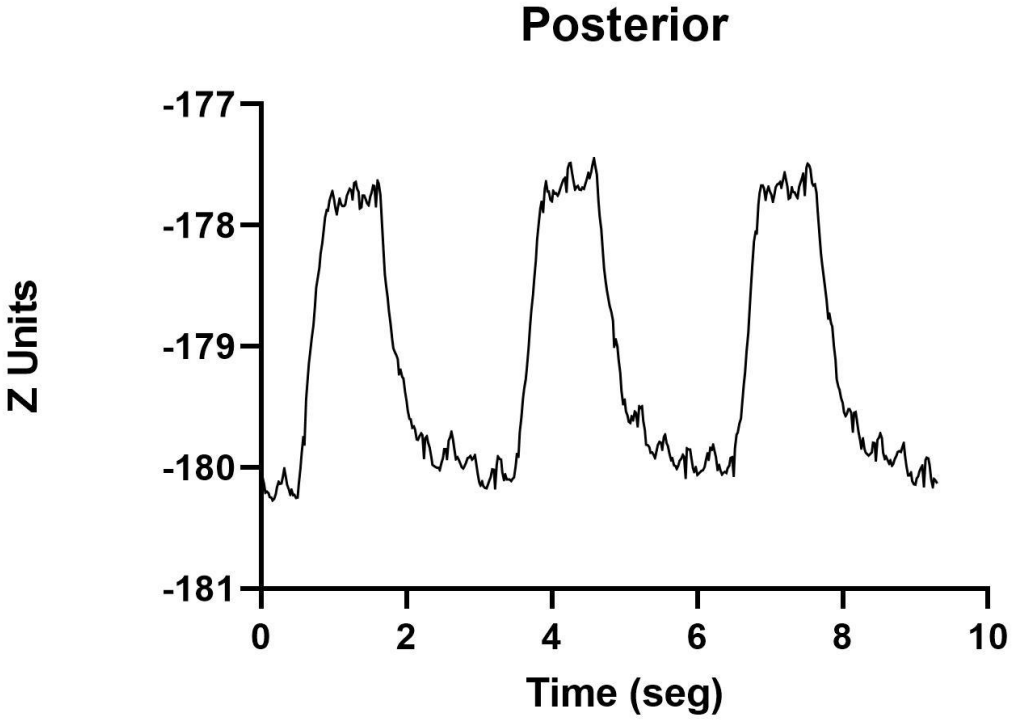

Figure E14

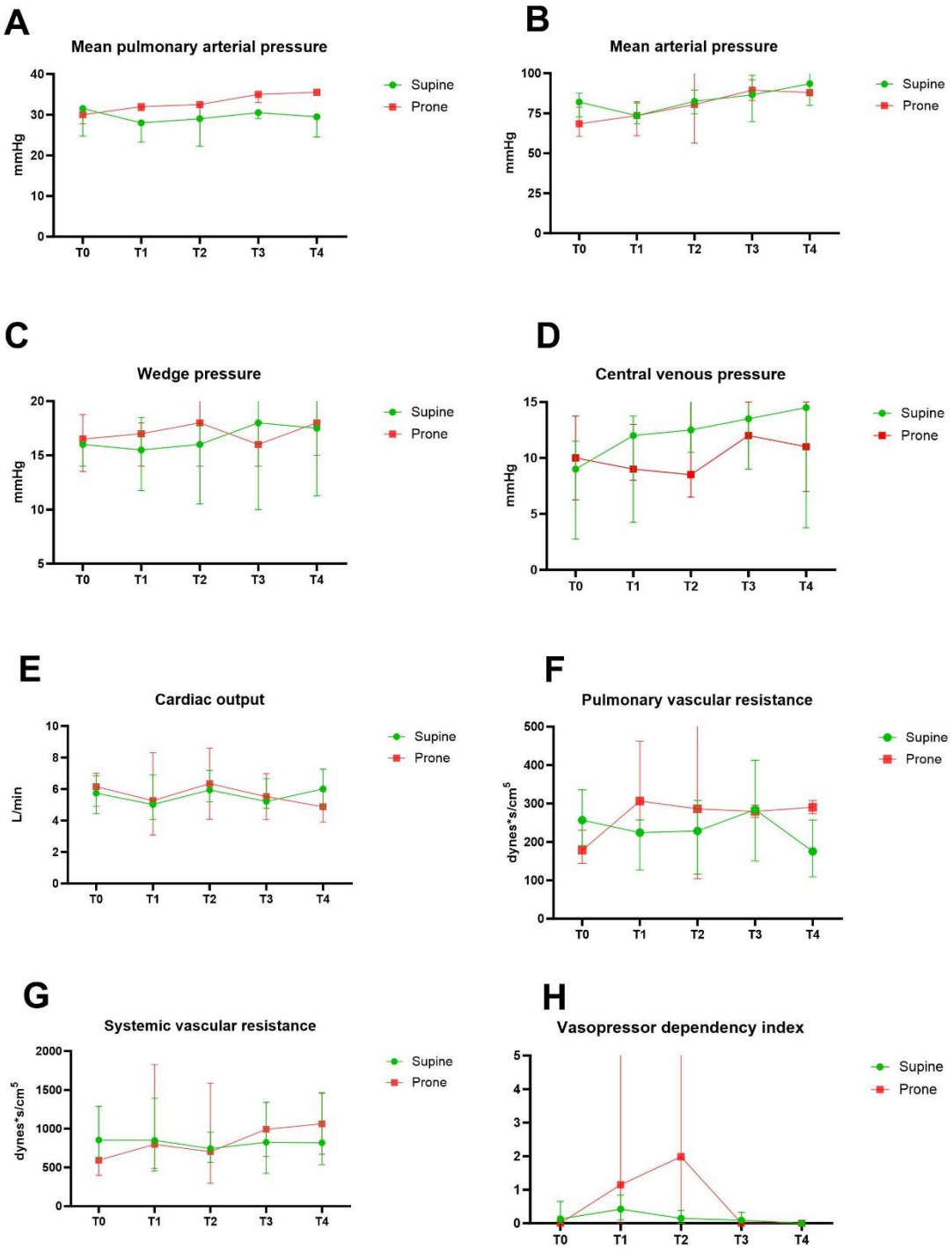
A
Mean pulmonary arterial pressure
mmHg
40
30
20
10
0
T0
T1
T2
T3
T4
Supine
Prone
B
Mean arterial pressure
mmHg
100
75
50
25
0
T0
T1
T2
T3
T4
Supine
Prone
C
Wedge pressure
mmHg
20
15
10
5
T0
T1
T2
T3
T4
Supine
Prone
D
Central venous pressure
mmHg
15
10
5
0
T0
T1
T2
T3
T4
Supine
Prone
E
Cardiac output
L/min
10
8
6
4
2
0
T0
T1
T2
T3
T4
Supine
Prone
F
Pulmonary vascular resistance
dynes*s/cm5
500
400
300
200
100
0
T0
T1
T2
T3
T4
Supine
Prone
G
Systemic vascular resistance
dynes*s/cm5
2000
1500
1000
500
0
T0
T1
T2
T3
T4
Supine
Prone
H
Vasopressor dependency index
5
4
3
2
1
0
T0
T1
T2
T3
T4
Supine
Prone

Figure E15

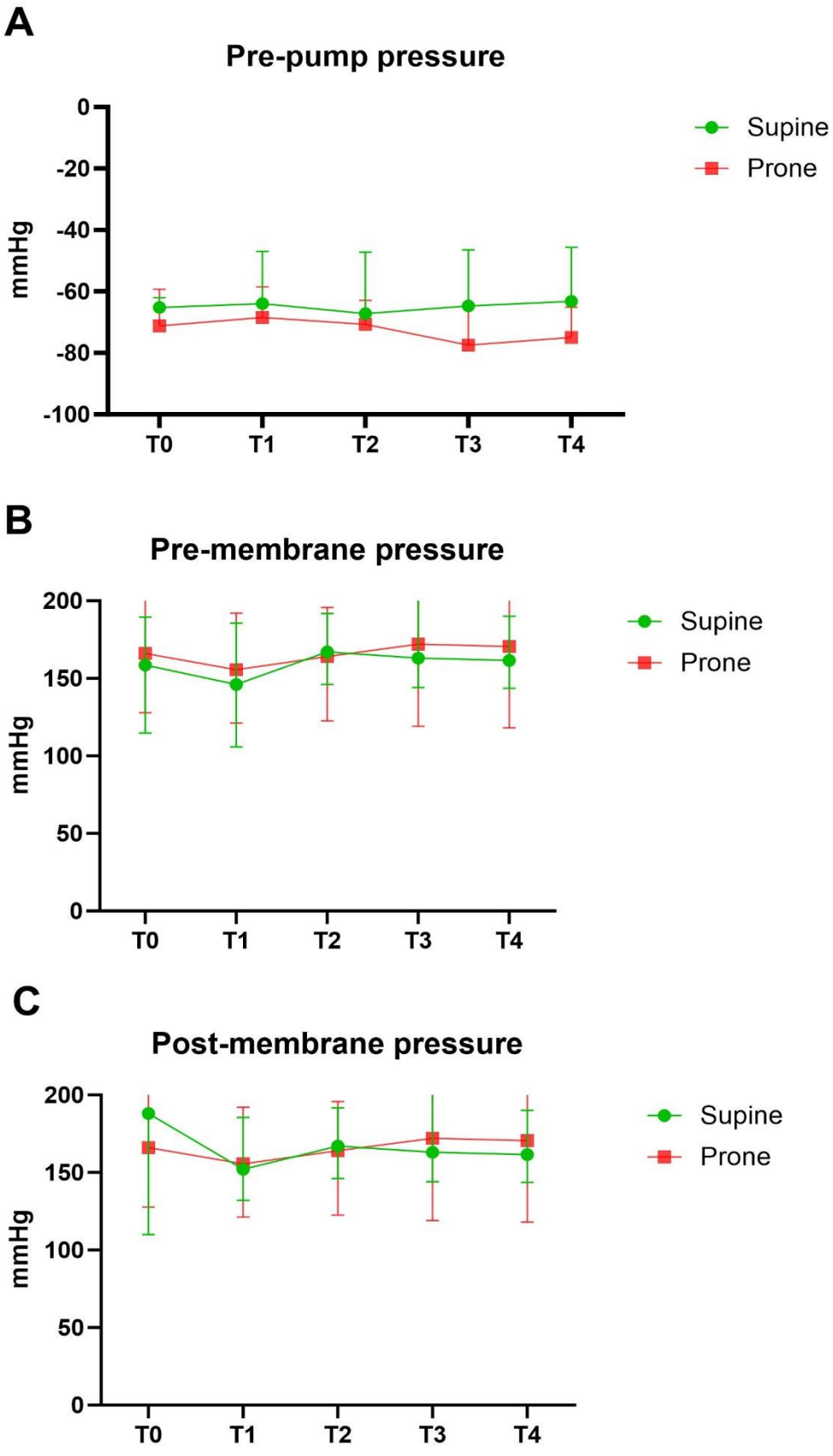
A
Pre-pump pressure
0
-20
-40
-60
-80
-100
mmHg
T0
T1
T2
T3
T4
Supine
Prone
B
Pre-membrane pressure
200
150
100
50
0
mmHg
T0
T1
T2
T3
T4
Supine
Prone
C
Post-membrane pressure
200
150
100
50
0
mmHg
T0
T1
T2
T3
T4
Supine
Prone

Figure E16

A

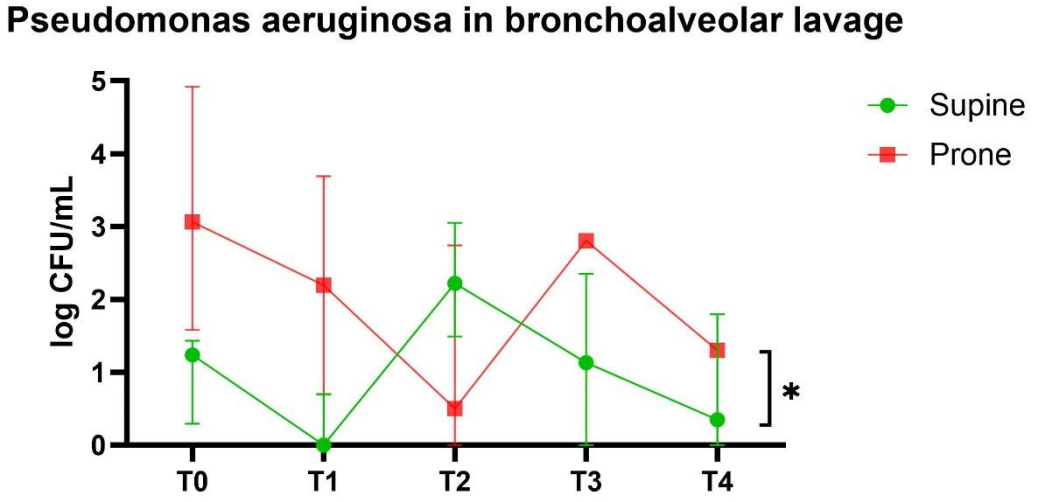

B

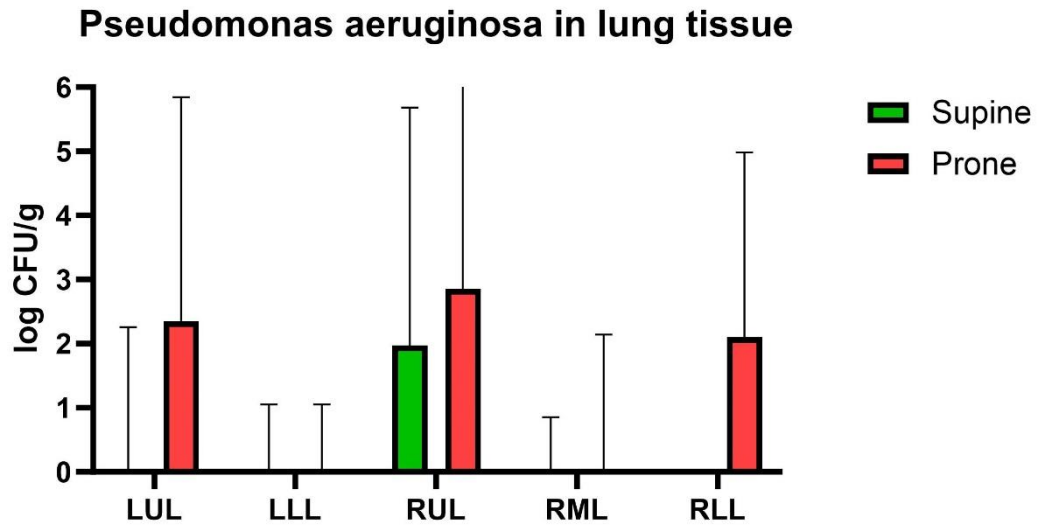

Figure Legends Supplemental

Figure E1. Evolution of driving pressure during the induction of severe ARDS.

p <0.0001

Timepoints correspond to key phases of the ARDS model: T–3 represents baseline, T–2 corresponds to the time of ARDS diagnosis, T–1 marks the moment when EOLIA inclusion criteria were met, and T0 indicates VV-ECMO initiation.

Abbreviations: ARDS, acute respiratory distress syndrome; VV-ECMO, veno-venous extracorporeal membrane oxygenation.

Figure E2. Evolution of extravascular lung water during the induction of severe ARDS.

p = 0.006

Timepoints correspond to key phases of the ARDS model: T–3 represents baseline, T–2 corresponds to the time of ARDS diagnosis, T–1 marks the moment when EOLIA inclusion criteria were met, and T0 indicates VV-ECMO initiation.

Abbreviations: ARDS, acute respiratory distress syndrome; VV-ECMO, veno-venous extracorporeal membrane oxygenation.

Figure E3. Evolution of the lung to respiratory system elastance ratio during the induction of severe ARDS.

p = 0.0003

Timepoints correspond to key phases of the ARDS model: T–3 represents baseline, T–2 corresponds to the time of ARDS diagnosis, T–1 marks the moment when EOLIA inclusion criteria were met, and T0 indicates VV-ECMO initiation.

Abbreviations: ARDS, acute respiratory distress syndrome; VV-ECMO, veno-venous extracorporeal membrane oxygenation.

Figure E4. Evolution of minute ventilation during the induction of severe ARDS.

p = 0.002

Timepoints correspond to key phases of the ARDS model: T–3 represents baseline, T–2 corresponds to the time of ARDS diagnosis, T–1 marks the moment when EOLIA inclusion criteria were met, and T0 indicates VV-ECMO initiation.

Abbreviations: ARDS, acute respiratory distress syndrome; VV-ECMO, veno-venous extracorporeal membrane oxygenation.

Figure E5. Evolution of arterial carbon dioxide tension ($PaCO_2$) during the induction of severe ARDS.

p = 0.005

Timepoints correspond to key phases of the ARDS model: T–3 represents baseline, T–2 corresponds to the time of ARDS diagnosis, T–1 marks the moment when EOLIA inclusion criteria were met, and T0 indicates VVECMO initiation.

Abbreviations: ARDS, acute respiratory distress syndrome; VV-ECMO, veno-venous extracorporeal membrane oxygenation; $PaCO_2$, arterial partial pressure of carbon dioxide.

Figure E6. Evolution of PaO_2/FiO_2 ratio during the induction of severe ARDS.

p = 0.0003

Timepoints correspond to key phases of the ARDS model: T–3 represents baseline, T–2 corresponds to the time of ARDS diagnosis, T–1 marks the moment when EOLIA inclusion criteria were met, and T0 indicates VV-ECMO initiation.

Abbreviations: ARDS, acute respiratory distress syndrome; VV-ECMO, veno-venous extracorporeal membrane oxygenation; PaO_2, arterial partial pressure of oxygen; FiO_2, fraction of inspired oxygen.

Figure E7. Evolution of positive end-inspiratory pressure during the induction of severe ARDS.

p <0.0001

Timepoints correspond to key phases of the ARDS model: T–3 represents baseline, T–2 corresponds to the time of ARDS diagnosis, T–1 marks the

moment when EOLIA inclusion criteria were met, and T0 indicates VV-ECMO initiation.

Abbreviations: ARDS, acute respiratory distress syndrome; VV-ECMO, veno-venous extracorporeal membrane oxygenation.

Figure E8. Evolution of respiratory system compliance during the induction of severe ARDS.

p = 0.0003

Timepoints correspond to key phases of the ARDS model: T–3 represents baseline, T–2 corresponds to the time of ARDS diagnosis, T–1 marks the moment when EOLIA inclusion criteria were met, and T0 indicates VV-ECMO initiation.

Abbreviations: ARDS, acute respiratory distress syndrome; VV-ECMO, veno-venous extracorporeal membrane oxygenation.

Figure E9. Evolution of shunt fraction during the induction of severe ARDS.

p <0.0001

Timepoints correspond to key phases of the ARDS model: T–3 represents baseline, T–2 corresponds to the time of ARDS diagnosis, T–1 marks the moment when EOLIA inclusion criteria were met, and T0 indicates VV-ECMO initiation.

Abbreviations: ARDS, acute respiratory distress syndrome; VV-ECMO, veno-venous extracorporeal membrane oxygenation.

Figure E10. Evolution of tidal volume during the induction of severe ARDS.

p <0.0001

Timepoints correspond to key phases of the ARDS model: T–3 represents baseline, T–2 corresponds to the time of ARDS diagnosis, T–1 marks the moment when EOLIA inclusion criteria were met, and T0 indicates VV-ECMO initiation.

Abbreviations: ARDS, acute respiratory distress syndrome; VV-ECMO, veno-venous extracorporeal membrane oxygenation; IBW, ideal body weight.

Figure E11. Evolution of physiological dead space (Enghoff) (Vd/Vt) during the induction of severe ARDS.

p = 0.007

Timepoints correspond to key phases of the ARDS model: T–3 represents baseline, T–2 corresponds to the time of ARDS diagnosis, T–1 marks the moment when EOLIA inclusion criteria were met, and T0 indicates VV-ECMO initiation.

Abbreviations: ARDS, acute respiratory distress syndrome; VV-ECMO, veno-venous extracorporeal membrane oxygenation; Vd/Vt, physiological dead space (Enghoff).

Figure E12. (A-C) Representative volumetric capnography recordings obtained during ARDS induction (panel A) and during VV-ECMO support (panels B and C). A: During ARDS induction, the volumetric capnography displays a preserved sigmoidal morphology, with a clearly identifiable phase I (airway dead space), a distinct phase II (transition between airway and alveolar gas), and a discernible phase III (alveolar plateau). Under these conditions, alveolar PCO_2 ($PACO_2$) and mixed expired CO_2 ($PECO_2$) are measurable, allowing calculation of both Bohr- and Enghoff-derived physiological dead space. Moreover, the volumetric capnography morphology permits discrimination between airway and alveolar components of physiological dead space based on the shape and phase transitions of the curve. B: During VV-ECMO support, the volumetric capnography shows a marked alteration of its morphology, with loss of the preserved sigmoidal shape. Phase I (airway dead space) remains identifiable; however, phase II is blunted and prolonged, and no discernible phase III (alveolar plateau) can be identified. Under these conditions, $PECO_2$ is extremely low but detectable, reflecting minimal pulmonary CO_2 elimination. In the absence of a clearly defined alveolar plateau, $PACO_2$ cannot be reliably identified, precluding the physiological application of Bohr's equation. Consequently, Enghoff-derived physiological dead space should be interpreted as a global index of ventilatory inefficiency, rather than a direct measure of alveolar dead space. Discrimination between airway and alveolar components of physiological dead space is limited by the attenuated alveolar CO_2 signal. C: In some VV-ECMO recordings, the volumetric capnography demonstrates no pulmonary CO_2 elimination, resulting in $PECO_2$ values of zero. When tidal

volume was lower than the baseline airway dead space volume and $PECO_2$ was zero, physiological dead space was assumed to be 100%.

Figure E13. (A–D) Regional electrical impedance tomography tracings showing anterior and posterior lung ventilation in prone and supine positions. A: anterior dependent region in the prone position; B: anterior non-dependent region in the supine position; C: posterior non-dependent region in the prone position; D: posterior dependent region in the prone position. In the anterior lung regions, EELZ differs between positions: panel A shows lower absolute EELZ compared with panel B. In the posterior lung regions, EELZ also differs between positions: panel C demonstrates higher EELZ values compared with panel D. Among the four panels, ΔZ was lowest in panel D and highest in panel B.

Figure E14. (A–H) Time courses of Mean Arterial Pulmonary Pressure (A), Mean Arterial Pressure (B), Wedge Pressure (C), Central Venous Pressure (D), Cardiac Output (E), Pulmonary Vascular Resistance (F), Systemic Vascular Resistance (E) and Vasopressor Dependency Index (H) throughout the experiment. A-H: no significant differences between groups. T0 corresponds to ECMO initiation (all animals in the supine position); T1, T2, T3, and T4 correspond to 12, 24, 36, and 48 hours after ECMO initiation, respectively. Animals in the prone position group were turned to the supine position at hours 22 (first session) and 46 (second session) after ECMO initiation; therefore, measurements at T2 and T4 were obtained in the supine position. Values are presented as median ± IQR.

Figure E15. (A-C) Time courses of Pre-pump Pressure (A), Pre-membrane Pressure (B) and Post-membrane Pressure (C), throughout the experiment. A – C: no significant differences between groups. T0 corresponds to ECMO initiation (all animals in the supine position); T1, T2, T3, and T4 correspond to 12, 24, 36, and 48 hours after ECMO initiation, respectively. Animals in the prone position group were turned to the supine position at hours 22 (first session) and 46 (second session) after ECMO initiation; therefore, measurements at T2 and T4 were obtained in the supine position. Values are presented as median ± IQR.

Figure E16. (A and B) Pseudomonas aeruginosa in bronchoalveolar lavage (A) and Pseudomonas aeruginosa in lung tissue (B). A: there was a significant increase in the burden of Pseudomonas aeruginosa in bronchoalveolar lavage ($p = 0.04$), but not in lung tissue (B). Values are presented as median ± IQR. *: $p < 0.05$ (*), $p < 0.01$ (**), and $p < 0.001$ (***).

References:

1. Enric Barbeta, Marta Arrieta, Ana Motos, Joaquim Bobi, Hua Yang, Minlan Yang, Giacomo Tanzella, Pierluigi Di Ginnatale, Stefano Nogas, Carmen Rosa Vargas, Roberto Cabrera, Denise Battaglini, Andrea Meli, Kasra Kiarostami, Nil Vázquez, Laia Fernández-Barat, Montserrat Rigol, Ricard Mellado-Artigas, Gerard Frigola, Marta Camprubí-Rimblas, Pau Ferrer, Daniel Martinez, Antonio Artigas, Carlos Ferrando, Miquel Ferrer, Antoni Torres. A long-lasting porcine model of ARDS caused by pneumonia and ventilator-induced lung injury. Crit Care. 2023 Jun 16;27(1):239.

2. Alessandro Protti, Davide T Andreis, Marta Milesi, Giacomo E Iapichino, Massimo Monti, Beatrice Comini, Paola Pugni, Valentina Melis, Alessandro Santini, Daniele Dondossola, Stefano Gatti, Luciano Lombardi, Emiliano Votta, Eleonora Carlesso, Luciano Gattinoni. Lung anatomy, energy load, and ventilator-induced lung injury. Intensive Care Med Exp. 2015;3(1):1–18.

3. Panigada M, Berra L, Greco G, et al.: Bacterial colonization of the respiratory tract following tracheal intubation-effect of gravity: an experimental study. Crit Care Med 2003; 31: 729-37.